Fluorescence correlation spectroscopy on electron transfer reactions : probing inter- and intramolecular redox processes

Sen, S.

Chapter 4

Observation of intramolecular electron-transfer reactions by fluorescence correlation spectroscopy: Photoinduced electron-transfer reaction between the label and the copper center

Abstract

A detailed investigation of the products of the labeling reaction of *wt* Cu azurin with the fluorescent dye ATTO655 has been performed. Fluorescence correlation spectroscopy was performed to understand the behavior of the labeled products. In this work, we have tried to understand the photoinduced electron-transfer (PET) reaction using two species: one labeled at the N-terminus and another one labeled at Lys122 position. Intramolecular photoinduced electron-transfer (PET) to the metal is observed when a redox metal ion occupies the active site, and the label is attached close enough to the metal center (at Lys122) and occurred in microsecond time scale. Two different mechanisms are equally likely to be involved in the electron-transfer event. In N-terminally labeled protein, the label is far away from the metal center and there is no PET reaction.

4.1 *Introduction*

Inter- and intramolecular electron transfer (ET) reactions have been a subject of research over the past few decades and several experimental and computation methods have been employed to investigate these. Application of redox proteins especially azurin, nitrite reductase, cytochrome P450 has tremendously enhanced the progress of this field. Single-molecule techniques appear eminently suited for the study of such enzymes at single-molecule level(*1*)(*2*)(*3*)(*4*)(*5*)(*6*)(*7*). To monitor the working of these oxido-reductases in detail, a novel FRET-based technique, FluoRedox had been developed(*8*)(*9*)(*10*)(*11*)(*12*). FluRedox technique has tremendously facilitated the detection of the redox state change due to the sensitivity of fluorescence detection. The technique used here depends on the labeling of the protein by dye molecules, the fluorescence of which overlaps spectrally with the absorption of the protein's redox center. When a change in the redox-state affects the absorption spectrum of the redox protein, the energy-transfer process between the dye and the metal center is affected and this leads to a change in the fluorescence intensity of the dye (see Chapter 1 for details).

In the studies reported so far it has been tacitly assumed that quenching of the dye fluorescence is brought about solely by FRET(*13*). However, the optically excited label may be deactivated by photo-induced electron transfer (PET) as well. Instances have been reported where van der Waals contact between dye label and amino acid side chains appears to promote PET(*14*)(*15*)(*16*)(*17*). Working along different lines, Gray and co-workers found that photo-excited Ru labels may transfer an electron across a protein at the sub-microsecond to millisecond time scale(*18*)(*19*)(*20*)(*21*). In this chapter, we investigate to what extent PET between dye label and redox center may occur in an oxido-reductase.

As the model system we have chosen the blue copper protein azurin labeled with ATTO655. The effect of the redox state of the Copper (Cu) on the PET reaction was explored by studying the labeled azurin in the oxidized and in the reduced form. The technique chosen to study the time dependence of the label emission is fluorescence correlation spectroscopy (FCS), a single-molecule technique that can be used to monitor diffusing fluorescent particles in dilute solutions. Probing small numbers of molecules at a time by FCS and statistical analysis of the data reveals dynamics otherwise obscured by ensemble averaging(*22*)(*23*)(*24*)(*25*). When combined with modern hard- and software, FCS allows for a time resolution in the ps range(*26*).

The intermolecular reaction between the label and the redox agents affects the FCS signal and has been discussed in the previous chapter. In the present study, we have investigated the intramolecular ET reaction between the label and copper center. Redox active components in solution like potassium hexacyanoferrate(II) and (III), which have been used in the present study, react with azurin by forming an encounter complex within which ET occurs on the time scale of 20-200 ms(*27*). This is much longer than the time an azurin molecule needs on average to traverse the confocal volume, which means that these reactions fall outside the observation window of the FCS experiments. The same is true when ascorbate is used as a reductant. Thus for the interpretation of FCS traces we need to consider the intramolecular ET between label and Cu and the intermolecular ET reactions between the label and the redox chemicals that were discussed in Chapter 3.

The results presented here provide detailed insight into the kinetics of the intra- and intermolecular PET reactions. Rate constants for the reactions were determined. The rate constants also demonstrate that the position of the label on the protein surface has to be selected carefully in order to get reliable information on the mechanistic behaviour of a labeled oxido-reductase.

4.2 *Materials and Methods*

4.2.1 *Chemicals and proteins*

Unless stated otherwise, chemicals were purchased from Sigma-Aldrich (Sigma-Aldrich Corp., St. Louis, USA) and used as received. Wild-type Cu-azurin from *Pseudomonas aeruginosa* were expressed and purified as previously described (Chapter 3 and ref. (*28*)). For the labeling of the protein with the dye ATTO655 (ATTO655 NHS ester, ATTO-TEC GmbH, Siegen, Germany) the supplier-provided protocol was used. Labeling resulted in a mixture of products that could be separated by ion exchange chromatography on a MonoQ column. The elution profile is shown in Fig. 4.1. Peaks 1-5 correspond with unlabeled azurin, azurin labeled at the N-terminus (Nt-CuAzu)(*29*), labeled at Lys122 (K122-CuAzu) (Fig. 4.2), Lys24 or Lys27 (not further investigated), and a doubly labeled species, respectively(*29*). For the experiments described in this study, N-terminally labeled and Lys122 labeled azurin were selected. They represent azurins

where the label is either far away from (29.1 Å) or relatively close to (18.5 Å) the Cu-site, respectively.

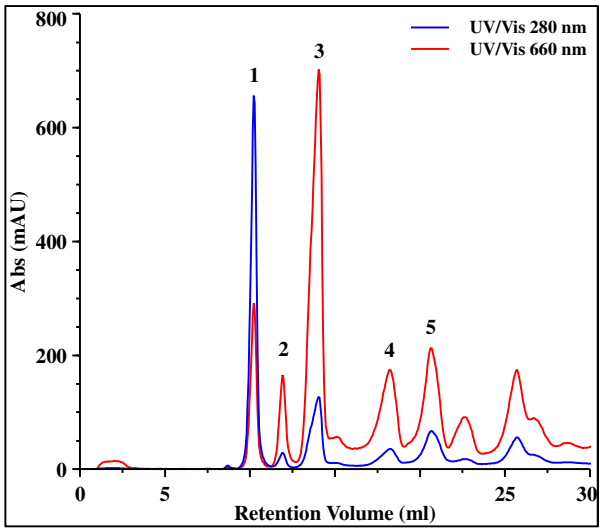

Figure 4.1: *Chromatogram showing the separation of dye-labeled CuAzurin species. The peaks are labeled from 1 through 5 and correspond with unlabeled azurin (1), N-terminally labeled azurin (2), Lys122 labeled azurin (3), a mixture of differently labeled species (4), and a doubly labeled species (5), respectively.*

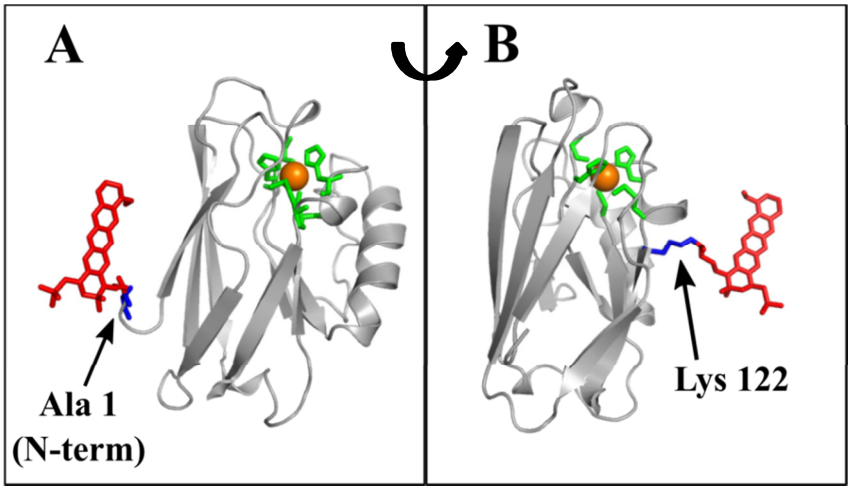

Figure 4.2: *Depiction of azurin (gray) modified with ATTO655 (red) on the two positions studied in the present work. The Cu ion and the 5 residues coordinating it are depicted, respectively, as an orange sphere and green sticks. A) Label linked to the N-terminal residue Ala1 (blue). B) Label attached to the side chain of Lys122 (blue). The figures were prepared in silico by using the available crystal structure of azurin (1AZU)(30) and the molecular structure of the label ATTO655. The molecule in panel B has been rotated counterclockwise over 90 ^{o} with respect to panel A around a vertical axis in the plane of the page.*

4.2.2 *UV/Vis absorption and fluorescence spectroscopy*

All optical absorption and fluorescence experiments on bulk solutions were carried out at room temperature in 100 mM HEPES pH 7.0 under stirring. UV/Vis absorption spectra were recorded on a Cary 50 Spectrophotometer (Agilent Technologies, Santa Clara, CA, USA) at a speed of 400 nm/min with a bandwidth of 2 nm and an interval of 1 nm between data points. With the use of a Cary Eclipse Spectrophotometer (Agilent Technologies, Santa Clara, CA, USA), emission spectra of fluorescently labeled azurin samples were recorded in the 600 – 800 nm range by exciting the sample at 590 nm. Excitation and emission slits were set to 5 nm band-pass and suitable optical filters were automatically selected by the instrument to minimize second order diffraction effects of the monochromator. The concentration of labeled protein ranged from 50-100 nM and the total volume of the sample used was 100 µl in a 3 windows, quartz glass ultra-micro cell for fluorescence measurements (HellmaAnalytics, Mullheim, Germany). The photomultiplier tube (PMT) voltage was adjusted during each experiment to avoid signal saturation. Redox switching was performed using sodium ascorbate and potassium hexacyanoferrate(III) as reducing and oxidizing agents respectively. The time traces of fluorescence switching for Nt-CuAzu and K122-CuAzu under redox conditions have been presented in Fig. 4.3. Details on the principles of fluorescence switching and "FluRedox" technique have been provided in Chapter 1.

4.2.3 *Sample preparation*

Details about the sample preparation have been provided in Chapter 3. Samples contained 57.0% sucrose (w/w) (viscosity 37.5 cP at 22^0C)(*31*). The final sample concentrations of labeled protein were around 0.4-0.8 nM. Manipulation of the redox potential of the solution was achieved by employing hexacyanoferrate (III), hexacyanoferrate (II) or ascorbate.

4.2.4 *FCS setup*

The FCS calibration measurements were carried out at room temperature on our home-built confocal setup equipped with Axiovert 100 inverted microscope (Carl Zeiss, Germany) and a high numerical aperture (NA) water immersion objective (60x water, NA 1.2, Olympus UPLSAPO). Excitation at 639 nm was provided by a pulsed diode laser head (LDH-P-C-635-B, PicoQuant GmbH, Berlin, Germany) driven by a picosecond laser driver (LDH-800-B,

PicoQuant GmbH, Berlin, Germany). The fluorescence from the sample was collected by the water objective and spatially filtered using a 50 µm pinhole. The fluorescence from the dye was

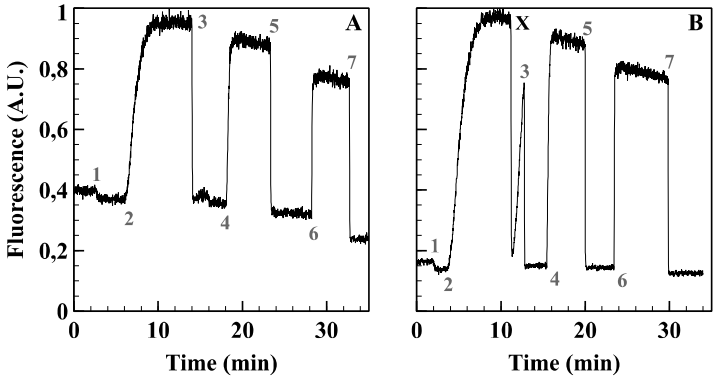

Figure 4.3: *Fluorescence switching experiments on fluorescently labeled copper azurin. The black numbers mark the addition of oxidant to the samples, whereas the gray numbers indicate the addition of reductant. A: N-terminally labeled azurin. B: azurin labeled at Lys122. The time points 1, 3, 5, and 7 correspond to the addition of 0.05, 1, 6, and 18 mM (final concentrations) of potassium ferricyanide to the sample, respectively. The time points 2, 4, and 6 correspond to the addition of 0.25, 1.5, and 4.5 mM of sodium ascorbate (final concentrations), respectively. At time point 'X' in panel B the added amount of ferricyanide was too low to completely oxidize the azurin. The subsequent addition (time point 3) was sufficient to complete the oxidation.*

passed through an emission filter (HQ 675/50m, Chroma Technology Corp., VT, USA), and focused onto a single-photon avalanche photodiode (SPCM-AQRH 14, Perkin Elmer Inc., USA). The signal from the diode was read out by using a TimeHarp200 counting board (PicoQuant GmbH, Berlin, Germany). The power used for the FCS measurements amounted to 20 µW, as measured after the objective, corresponding to a specific power of ~7.0 kW/cm^2 at the sample. The acquisition of the data was performed in the Time-Tagged Time Resolved Single Photon Mode (t3r) using the software package SymPhoTime from PicoQuant, Germany and FCS experiments were performed with sample volume ~80-100 µl. A schematic diagram of the FCS setup has been displayed in Fig. 4.4.

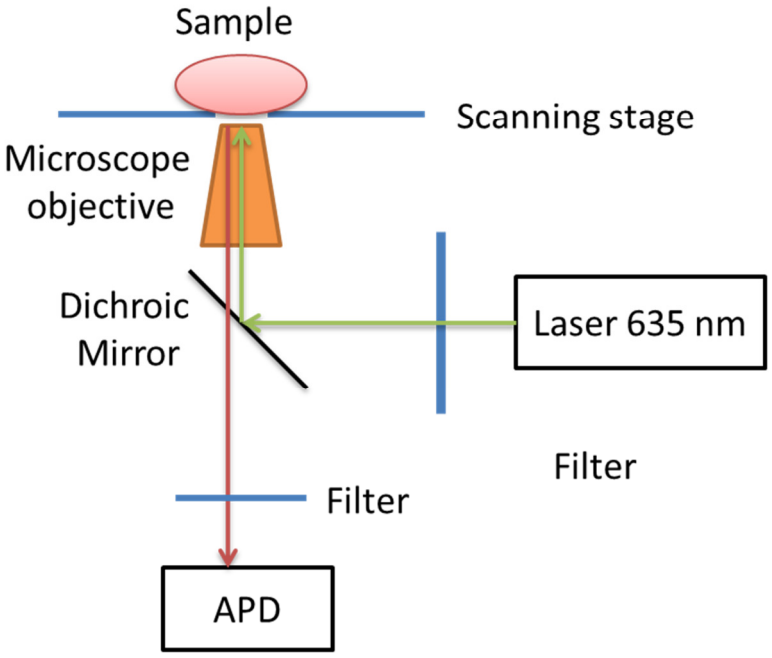

Figure 4.4: *Schematic representation of the experimental setup. The laser light (excitation wavelength: 635 nm) is transmitted through the narrow-band filter and reflected from the dichroic mirror through the objective. The emission light is collected by the same objective, transmitted through the dichroic mirror and the emission filter, and then focused on the avalanche photodiode (APD).*

4.2.5 *FCS data analysis*

After acquisition of the data the time correlated single photon counting (TCSPC) histogram was built and fitting was performed after narrowing down the time window of the TCSPC decay. Based on the fitted values, the software generated a set of filter functions, which were subsequently used by the software to select the photons for the calculation of the autocorrelation function (ACF), $G(\tau)$. The functions were analyzed by fitting to the following equation:

$$G(\tau) = G(0) \cdot G_{diff}(\tau) \cdot G_1(\tau) \cdot G_2(\tau) \qquad (4.1)$$

where $G(0)$ is given by

$$G(0) = \frac{1}{\langle N \rangle} = \frac{1}{c \cdot V_{eff} \cdot N_A} \qquad (4.2)$$

with $\langle N \rangle$ the average number of particles in the probe volume, c the sample concentration, V_{eff} the effective probe volume, and N_A Avogadro's constant. V_{eff} amounted to 1.1-2.3 fL depending

on conditions (Chapter 2 for more details).

Equation (1) is composed of three terms: a diffusive term, $G_{diff}(\tau)$ that describes the diffusion of molecules in solution due to Brownian motion, and two kinetic terms, $G_1(\tau)$ and $G_2(\tau)$, that relate to zero-order reactions such as fluorophore blinking or monomolecular chemical reactions like deprotonation or electron transfer (ET). $G_{diff}(\tau)$, $G_1(\tau)$ and $G_2(\tau)$ are given by

$$G_{diff}(\tau) = \left(1 + \frac{\tau}{\tau_D}\right)^{-1} \cdot \left(1 + \frac{\tau}{k^2 \tau_D}\right)^{-1/2} \qquad (4.3)$$

$$G_1(\tau) = \frac{(1 - F_1 + F_1 e^{-\tau/\tau_1})}{(1 - F_1)} \qquad (4.4)$$

$$G_2(\tau) = \frac{(1 - F_2 + F_2 e^{-\tau/\tau_2})}{(1 - F_2)} \qquad (4.5)$$

where τ_1 and τ_2 are the decay times of two independent zero-order reactions, and F_1 and F_2 are the corresponding fractions of molecules in the dark state, respectively.

Specific cases, to be described below, required the inclusion of one or two zero-order reactions, *i.e.*, $G_1(\tau)$ or both, $G_1(\tau)$ ànd $G_2(\tau)$, in the fitting procedure to obtain a satisfactory fit. $G_2(\tau)$, or both $G_1(\tau)$ ànd $G_2(\tau)$, were omitted when their inclusion in the fitting procedure gave no significant improvement of the fit. The fitting of the autocorrelation data was performed in GraphPad Prism 5 or 6.05 (GraphPad Inc., USA). The quality of the fits was judged by visual inspection of the residuals.

4.2.6 Fluorescence lifetime data acquisition

For the acquisition of fluorescence lifetime data the sample (~80 µl) was deposited on a glass slide and covered with the cap of a polypropylene test tube to prevent evaporation of the solvent during the measurements. A new cap was used for each measurement to prevent sample cross-contamination. The focus was set at a distance of 20 µm from the upper surface of the glass coverslip to prevent detection of fluorescence from surface-adsorbed molecules. The laser power for the measurements was adjusted by using a neutral density filter in front of the laser head and it was set at 20 µW (7.0 kW/cm^2, resolution of the setup ~300 nm), as measured at the

microscope objective. For power-dependence measurements, 6 different values of power were chosen ranging from 1 to 80 μW, as measured after the microscope objective. For each experimental condition, time traces were recorded for durations varying from 5 to 10 minutes, depending on the conditions of the experiment. Sample concentration was kept around 1 nM in order to lower the probability of having more than one molecule at the time in the confocal volume. The raw data were stored as time-tagged time-resolved (t3r) data file and subsequently elaborated by using the SymPhoTime software package.

4.3 *Results and discussion*

4.3.1. *Lifetimes of labeled azurin*

From the photon statistics, it is possible to extract information about the lifetimes of labeled Cu azurin under redox conditions. To estimate lifetimes, the decay curves could only be fitted with a double exponential function. The functions are given as

$$f = A_0 + A_1.\exp(-t/\tau_1) + A_2.\exp(-t/\tau_2) \qquad (4.6)$$

where, A_1 , A_2 and are the amplitudes and τ_1, τ_2 are the lifetimes of two processes present in solution and A_0 represents a local background. In our experiments, τ_1 displayed the lifetime of the dye and was found to be in the order of few nanoseconds, which is significantly longer than the instrument response function which is in the order of ps. We compared the amplitudes of A_2 and τ_2 with A_1 and τ_1. The contributions of A_2 and τ_2 for a second process were found to be negligible compared to A_1 and τ_1. τ_1 is the major component of the excited molecule. The second process can be originated from other factors e.g. interaction between dye molecules, adsorption, different rates of molecular rotation (*32*)(*33*). Under oxidising condition, the lifetime (τ_1) of the labeled Cu azurin is 1.8 ns whereas the lifetime is increased to 2.7 ns under reducing conditions. The time correlated single-photon count (TCSPC) decay curves at oxidizing and reducing conditions have been displayed in Fig. 4.5.

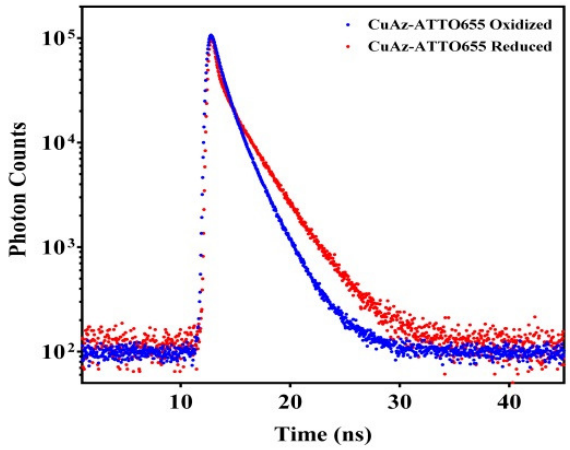

***Figure 4.5**: TCSPC decay of Cu azurin labeled with ATTO655 in sucrose in oxidizing and reducing conditions. It is possible to see the different slope of the lifetime decay when the protein is oxidized (blue) as compared to the reduced protein (red). The lifetime shortening is associated with FRET from the dye to the oxidized Cu center.*

4.3.2 *N-terminally labeled CuAzu (Nt-CuAzu)*

4.3.2.1 *Oxidizing conditions*

Fluorescence time traces of solutions of N-term-CuAz in 57% (w/w) sucrose were recorded in the presence of varying amounts (0-500 μM) of oxidant (potassium hexacyanoferrate (III)). 10-20 different concentrations of oxidant were analyzed. Examples of the experimentally observed autocorrelation functions have been provided for a few concentrations of hexacyanoferrate (III) (Fig. 4.6). Diffusion times are in the range of 10-12 ms. The diffusion times N-term-CuAz are good agreement with τ_D values of labeled ZnAzurin (12±2 ms, page 45). It is also clear from Fig. 4.6 (A-E) that the label is not affected by the added oxidant.

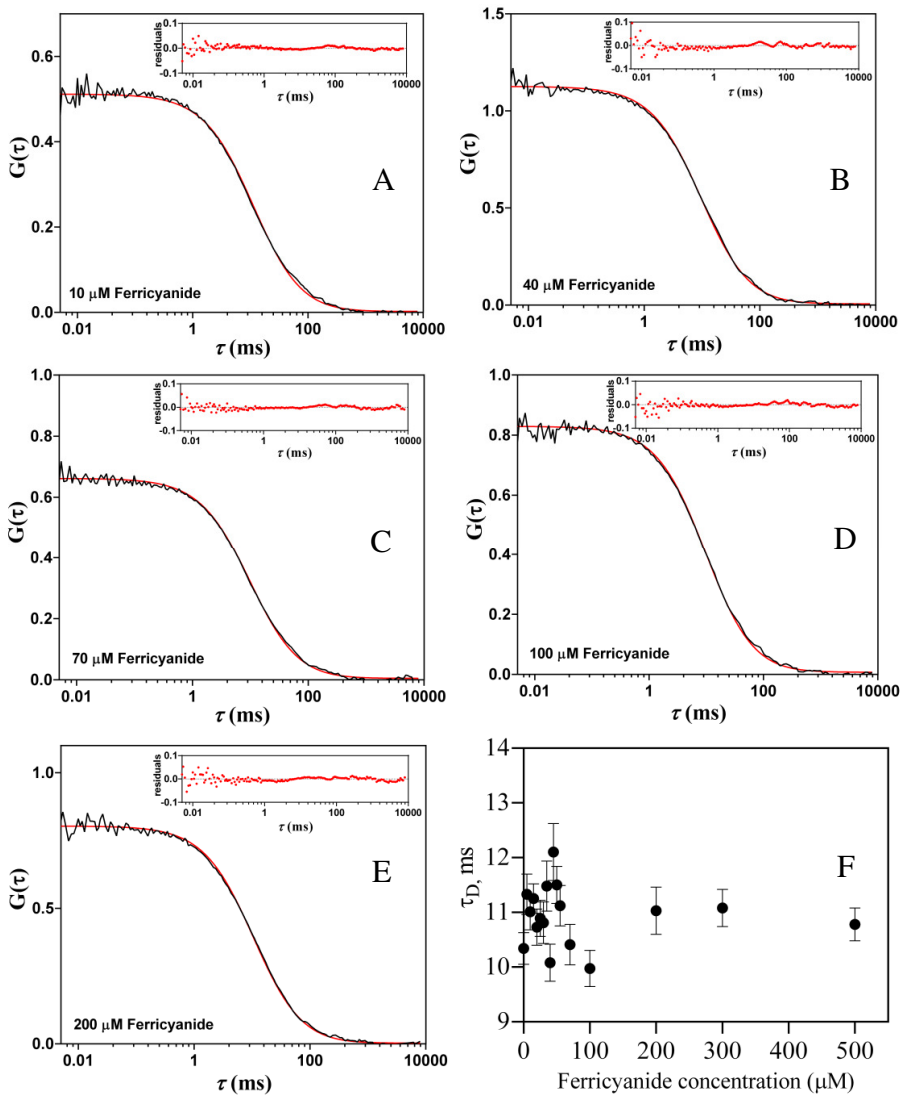

Figure 4.6: *Experimentally observed ACFs of Cu azurin labeled at N-terminus with ATTO655 for samples containing 10 (A), 40 (B), 70 (C), 100 (D) and 200 (E) potassium hexacyanoferrate (III) (top to bottom). The red lines are fits according to Eqn. 3.1 $G(\tau) = G(0).G_{diff}(\tau)$. The insets show the residuals of the fit. (F) Diffusion times derived from the fits for various concentrations of hexacyanoferrate (III).*

4.3.2.2 *Reducing conditions*

The observations are different when reducing conditions apply. The data obtained for N-term CuAzurin when titrated with potassium hexacyanoferrate (II) or sodium ascorbate were fitted with $G(\tau) = G(0).G_{diff}(\tau)$, but the residuals exhibited a noticeable non-random component. Similar to ZnAz, τ_D varied strongly with reductant concentrations (Fig. 4.7). Hence, they were fit

with the Eqn. 3.4 $G(\tau) = G(0).G_{diff}(\tau).G_1(\tau)$ with diffusion time fixed at 12 ms. The values of F_1 and τ_1 varied with reductant concentrations (Fig. 4.8).

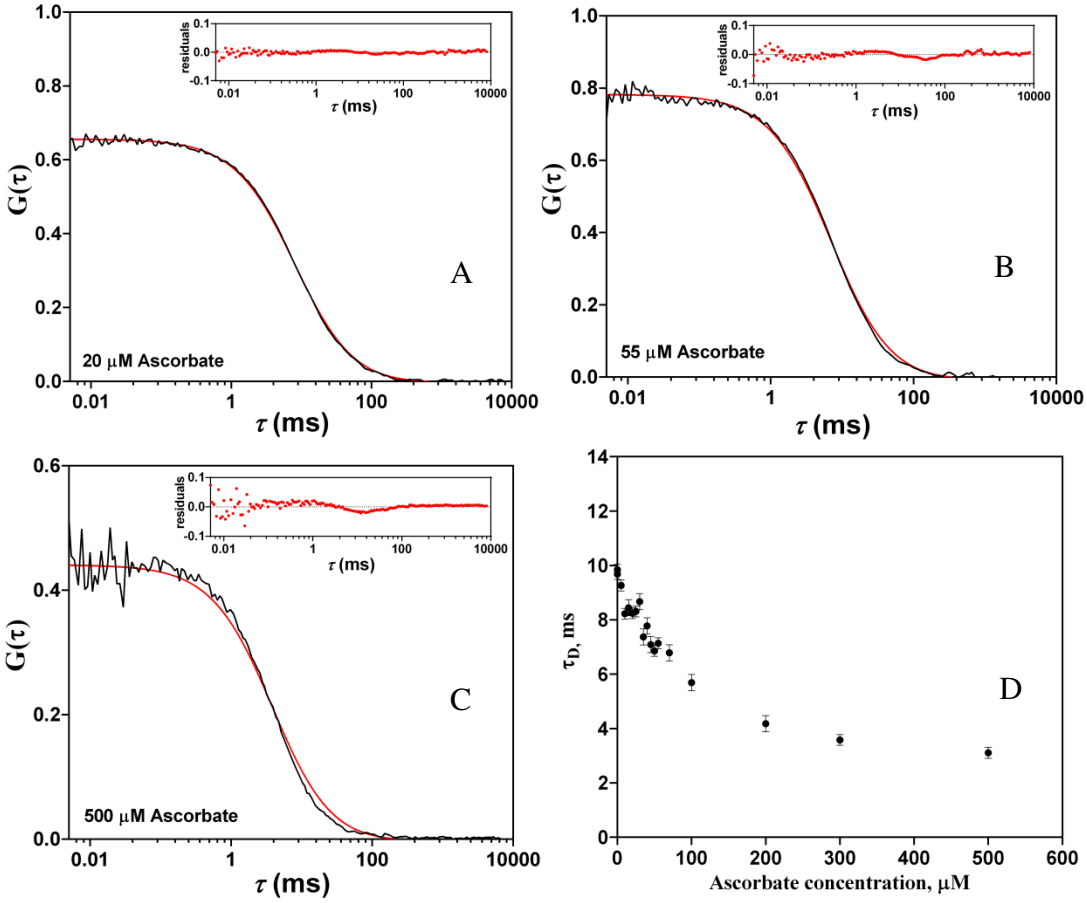

Figure 4.7: *Experimentally observed ACFs of Cu azurin labeled at the N-terminus with ATTO655 for samples containing 20 (A), 55 (B) and 500 (C) µM ascorbate. The insets are the residuals of the fit. The red lines are fits according to Eqn. 3.1 $G(\tau) = G(0).G_{diff}(\tau)$. (D) Diffusion times derived from the fits for various concentrations of ascorbate.*

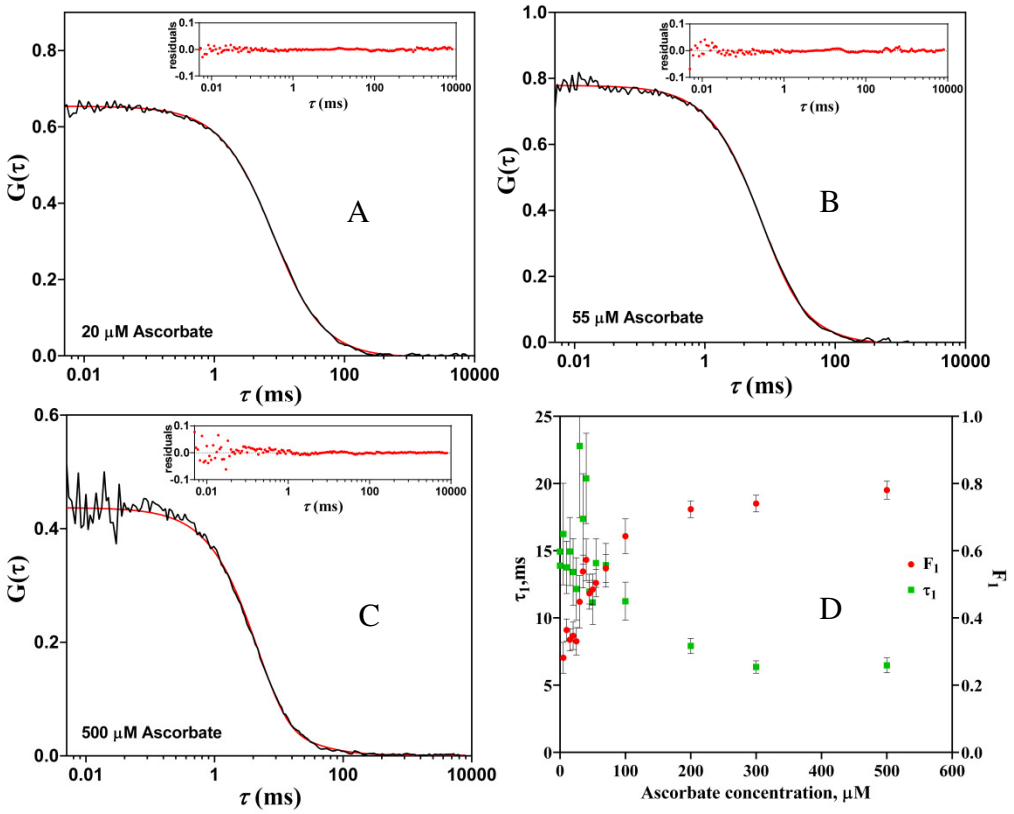

Figure 4.8: *Experimentally observed ACFs of Cu azurin labeled at the N-terminus with ATTO655 for samples containing 20 (A), 55 (B) and 500 (C) μM ascorbate. The red lines are fits according to Eqn. 3.4* $G(\tau) = G(0).G_{diff}(\tau).G_1(\tau)$ *with* $\tau_D = 12$ *ms. The insets show the residuals of the fit. (D) Parameters obtained from the fits. The green squares and red dots show the values for* τ_1 *and* F_1*, and correspond with left and right y-axis, respectively. Vertical bars denote 95% confidence intervals.*

It was clear again that the label undergoes transitions between a bright and a dark state in presence of reducing agents. Hence, the formalism which was discussed for ZnAz, was also applied for analyzing F_1 and τ_1 for this species. The dependence of $k_f = F_1/\tau_1$ and $k_b = (1-F_1)/\tau_1$ on reductant concentrations is illustrated by Scheme 4.1. k_f will be linearly proportional to the reductant concentrations. The values of $k_r f(I)$ and k_b (rate constant for the back oxidation of the label) are gathered in Table 4.1.

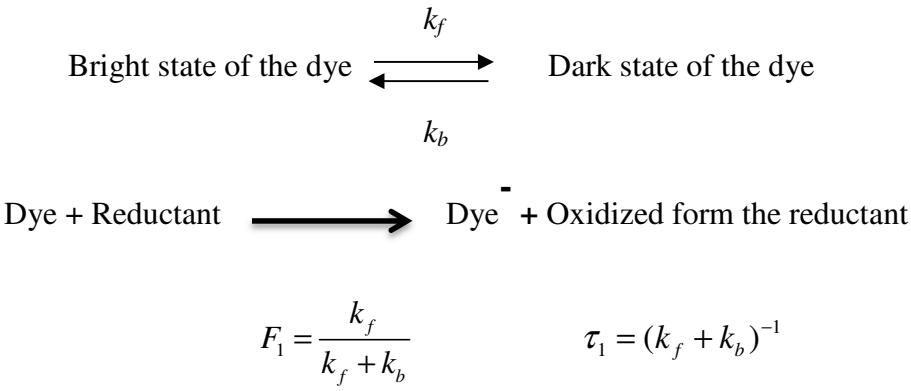

Scheme 4.1: *Schematic representation of photoinduced processes of the label. The label ATTO655 cycles between the bright and dark states under reducing conditions. The expressions of F_1 and τ_1 as function of k_f and k_b are displayed.*

4.3.3 K122-CuAz

4.3.3.1 *Oxidizing conditions*

When titrating K122-CuAz with hexacyanoferrate(III), the observed ACFs could not be fit adequately with the equation containing a single diffusion term (Fig. 4.9) and a two-term function with $G_{diff}(\tau)$ and $G_1(\tau)$ was needed to fit the data properly (Fig. 4.10). After fitting with two terms, we still observed inadequate fitting of ACFs for few concentrations of oxidants. Considering a third term $G_2(\tau)$ in FCS equation could not make any improvement of the fitting of the ACFs.

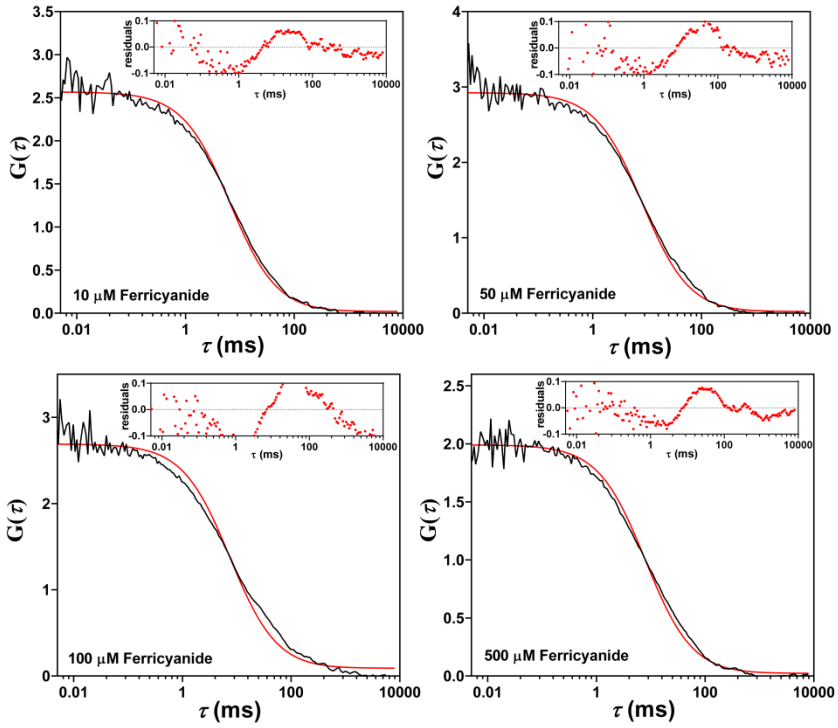

Figure 4.9: *Examples of experimentally observed ACFs of Cu azurin labeled at K122 position with ATTO655. Data sets were obtained on samples containing 10, 50, 100 and 500 µM hexacyanoferrate (III). The red lines are the fits according to Eqn. 3.1 $G(\tau) = G(0).G_{diff}(\tau)$. The insets show the residuals of the fit.*

It was clear, therefore, that next to the diffusion term ($G_{diff}(\tau)$) only a one term ($G_1(\tau)$) is needed to fit the experimental ACFs. After analysis, both F_1 and τ_1 appeared independent of the ferricyanide concentration with $F_1 = 0.17$ and $\tau_1 = 1.1$ ms (Fig. 4.11). This blinking reaction was not observed in the case of the Zn containing protein and so the Cu center must be involved in this reaction. Moreover, the blinking is also absent in the N-terminally labeled CuAz, which must mean that the distance between the Cu and the label is a critical factor (29.1 Å for N-term-Az vs. 18.5 Å for K122-Az). These are strong indications that intramolecular ET from the excited label to the Cu^{2+} site, and back, is responsible for the observed blinking, according to Scheme 4.2.

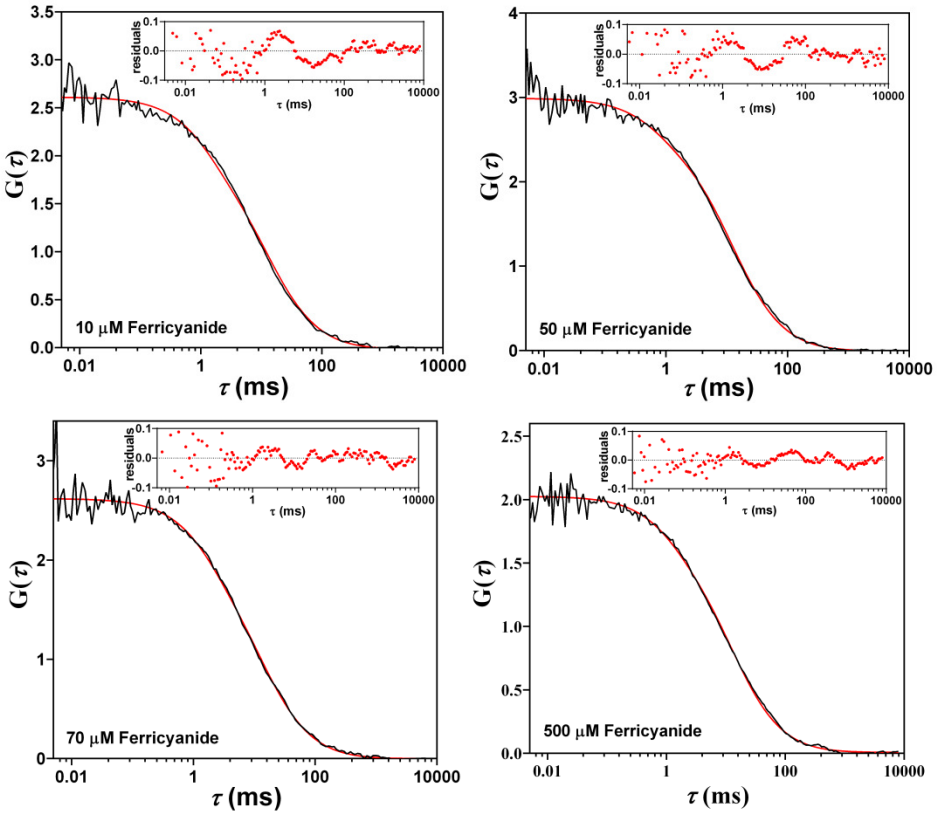

Figure 4.10: *Examples of experimentally observed ACFs of Cu azurin labeled at K122 position with ATTO655. Data sets were obtained on samples containing 10, 50, 70 and 500 μM hexacyanoferrate (III). The red lines are the fits according to Eqn. 3.4* $G(\tau) = G(0).G_{diff}(\tau).G_1(\tau)$ *with* $\tau_D = 12$ *ms. The insets show the residuals of the fit.*

$$LCu(II) \underset{k_{10}}{\overset{k_{01}}{\rightleftharpoons}} L^{*}Cu(II) \xrightarrow{k_1^{f}} L^{+}Cu(I) \xrightarrow{k_1^{b}} LCu(II)$$

Scheme 4.2: *Light induced ET reactions in oxidized CuAz. LCu symbolizes the labeled azurin molecule in which the Cu is in the reduced or oxidized form (Cu(I) or Cu(II), respectively) and the label, L, is excited or oxidized (L* or* L^+*, respectively). The rates for intramolecular ET from L* to Cu(II) and from Cu(I) to* L^+ *are denoted by* k_1^f *and* k_1^b *.*

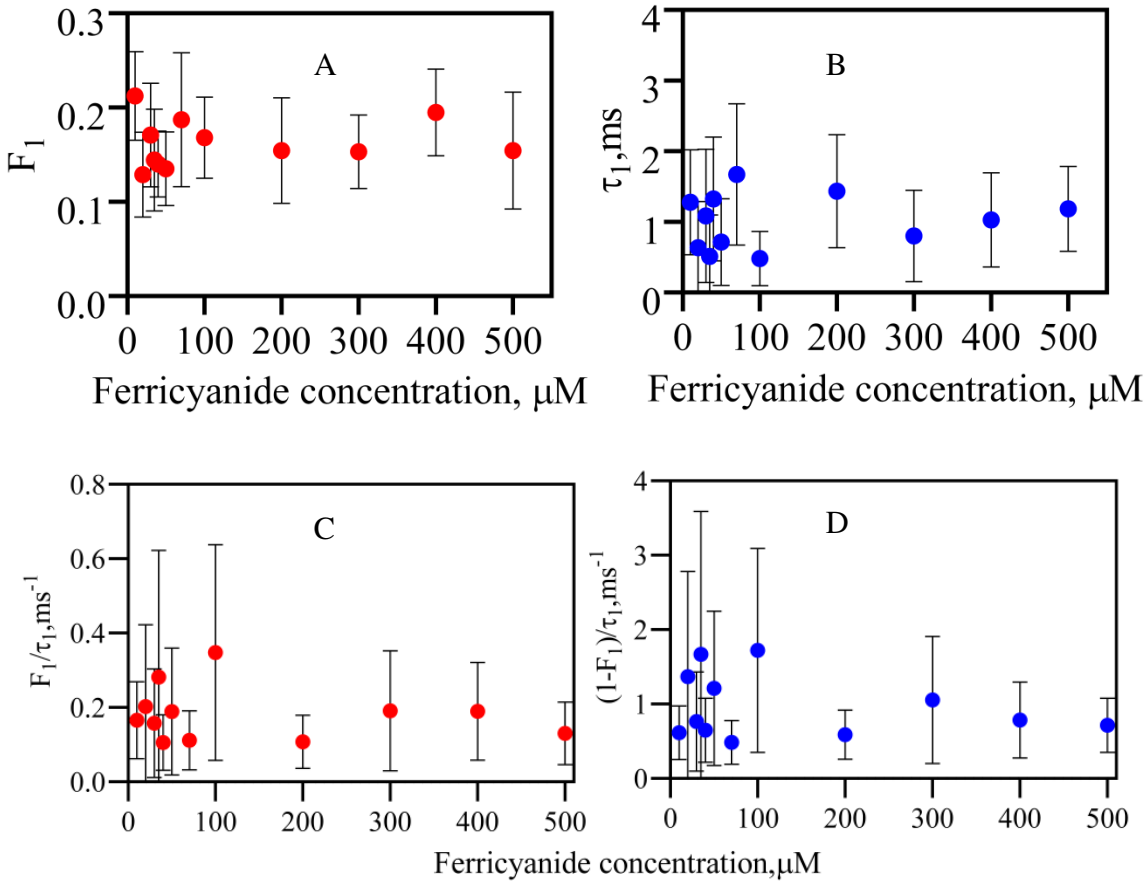

Figure 4.11*: (A) and (B): Parameters (F_1 and τ_1) obtained by fitting the ACFs of K122 labeled Cu azurin as a function of the concentration of added hexacyanoferrate (III). The equation used for the fits was $G(\tau) = G(0).G_{diff}(\tau).G_1(\tau)$ with τ_D =12 ms. The red and blue dots show the values for F_1 and τ_1. Vertical bars denote 95% confidence intervals. (C) and (D): $F_1/\tau_1 = k^f$ and $(1-F_1)/\tau_1 = k^b$ are plotted as a function of potassium hexacyanoferrate (III) concentrations. Vertical bars are the 95% confidence intervals. The ACFs were fitted the Eqn. 3.4 $G(\tau) = G(0).G_{diff}(\tau).G_1(\tau)$ with τ_D = 12 ms.*

Consistent with the intramolecular character of the reaction, neither F_1 nor τ_1 appears to depend on the concentration of oxidant (Fig. 4.11 A-B). Following the same formalism as applied for ZnAz (Chapter 3), one can obtain

$$F_1/\tau_1 = f(I)\ k_1^f \quad \text{and}$$

$$(1-F_1)/\tau_1 = k_1^b$$

In oxidized azurin the label fluorescence is partly quenched by the Cu center and the

fluorescence life time is shortened to 1.8 ns (Fig. 4.5). It leads to *f(1)*= 3.2×10^{-3}. With F_1 = 0.17 and τ_1= 1.1 ms, one obtains $k_1^f = 4.8\times10^4$ s^{-1} and $k_1^b = 7.5\times10^2$ s^{-1}.

The rates can be used to extract a value for the reorganization energy of the ET reaction. Applying Marcus theory [see ref. (*19*)(*34*)(*35*)(*36*) and references contained therein] and assuming that the reorganization energies and the electronic coupling elements are the same for the forward and backward ET reactions one obtains

$$\ln(k_1^f / k_1^b) = [(\Delta G_b+\lambda)^2 - (\Delta G_f+\lambda)^2]/(4\lambda kT) \qquad (4.7)$$

with ΔG_f and ΔG_b the driving forces for the forward and backward ET reactions, respectively, and λ the reorganization energy. The driving forces, ΔG can be estimated with the Rehm-Weller equation(*37*)

$$\Delta G_f = eE_{D^+/D} - eE_{A/A^-} - \Delta G_{0,0} + (n_A - n_D - 1)\frac{e^2}{\varepsilon d} \qquad (4.8)$$

which describes the driving force ΔG for the ET by a donor (*D*) to an acceptor (*A*) with $E_{D^+/D}$ and E_{A/A^-} denoting the midpoint potentials of donor and acceptor, respectively. An analogous expression holds for ΔG_b. Here, either the donor or the acceptor is optically excited with $\Delta G_{0,0}$ denoting the energy of the corresponding optical *0-0* transition. In Eqn. (4.8), *e* denotes the electron charge, *d* the distance between donor and acceptor, ε the dielectric constant and n_A and n_D the charges of acceptor and donor in units of |*e*|, respectively(*37*). For ATTO 655 the following values were used: $E_{ATTO^+/ATTO}$ = 1.55 V (vs NHE) and $\Delta G_{0,0}$ = 1.86 eV(*17*). The charges on label and Cu are n_{ATTO} = 0, $n_{Cu(II)}$=2. The midpoint potential of azurin at pH 7 is 0.31 V (vs NHE)(*38*)(*39*). This leads to driving forces of ΔG_f = -0.476 eV and ΔG_b = -1.384 eV for the reactions shown in *Scheme 4.2*. The values chosen for *d* and ε were *d* =10 Å and ε = 10, respectively (For our calculation, we set the distance (*d*) between donor and acceptor at 10 Å, which is the distance between the copper and the aromatic part of the label when ATTO655 moiety is modelled as lying against the protein surface in the K122 labeled azurin. In this configuration, the effective ε will be intermediate between that of pure protein (ε = 4) and that of water (ε = 86), and for the calculation purposes, we set ε at 10). Insertion into Eqn. 4.7 and solving for λ leads to λ= 0.75 eV. This value is slightly less than the theoretical value given by

the average of the known reorganization energies of ATTO655 and azurin (1.2 eV(*40*)(*41*) and 0.7(*42*) eV respectively).

4.3.3.2 *Reducing conditions*

Under reducing conditions an extra decay appeared in the ACF of K122-CuAz in the sub-millisecond time range. These curves could not be fitted with FCS equation containing two terms $G_{diff}(\tau)$ *and* $G_1(\tau)$ (Fig. 4.12). Only the use of a three-term correlation function (Eqn. (4.1)-(4.5), τ_D fixed at 12 ms) resulted in satisfactory fits (Fig. 4.13). The amplitudes F_1 and F_2, and the corresponding correlation times, τ_1 and τ_2 are presented in Fig. 4.14 (reductant: ascorbate), and Fig. 4.15 (reductant: hexacyanoferrate (II)) as a function of reductant concentrations.

As clear from Fig. 4.12 and 4.13, K122-labeled CuAz is involved in a reaction that occurs on a time scale of 10-100 µs. Similar to the preceding case this reaction is ascribed to intramolecular ET, this time from the Cu^+ site to the excited label and back (Scheme 4.3).

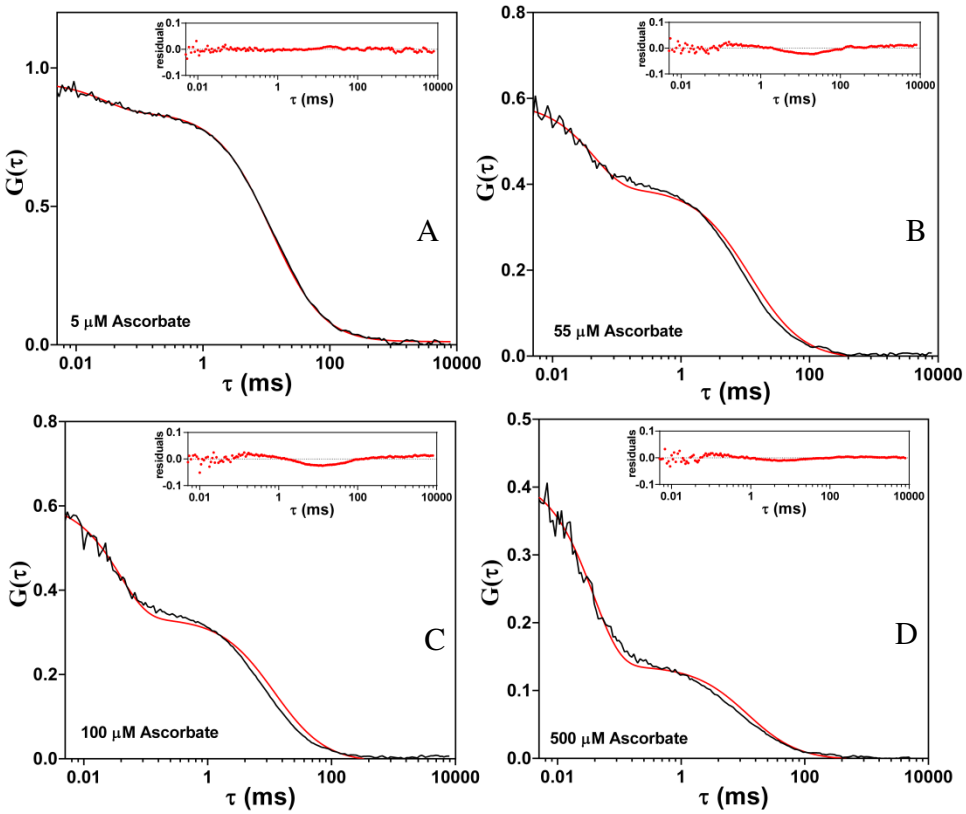

Figure 4.12: *Experimentally obtained ACFs of Cu azurin labeled at K122 position with ATTO655 for samples containing 5 (A), 55 (B), 100 (C) and 500 (D) µM ascorbate. The red lines are fits according to Eqn. 3.4* $G(\tau) = G(0).G_{diff}(\tau).G_1(\tau)$ *with* τ_D *=12 ms. The residuals of the fits in the insets show unsatisfactory fitting of the ACFs.*

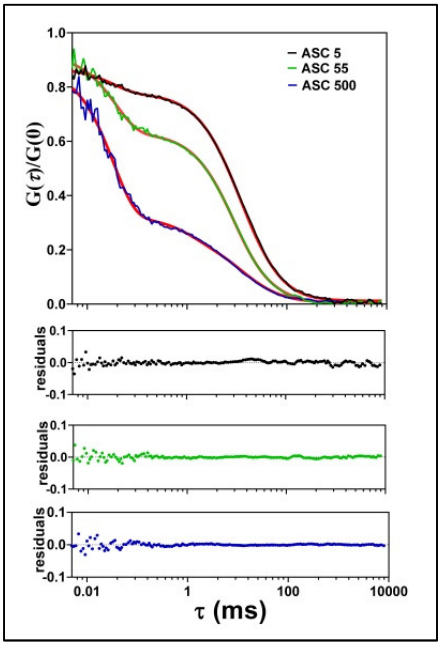

Figure 4.13: *(A) ACFs of Cu azurin labeled at K122 with ATTO655 together with plots of the residuals (below). Samples contained 5 (black), 55 (green) and 500 (blue) μM of ascorbate. The lines represent the experimentally observed ACFs. The red lines are fits according to Eqn. 4.1 with* $G(\tau)/G(0) = G_{diff}(\tau)\, G_1(\tau)\, G_2(\tau)$ *with* $\tau_D = 12$ *ms.*

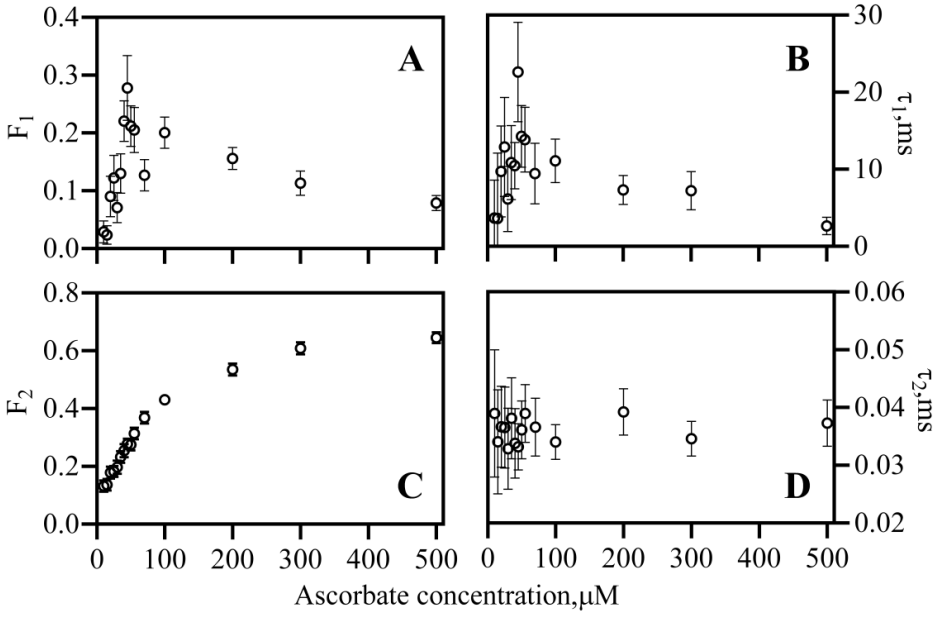

Figure 4.14: *Parameters obtained from the fits of the ACFs of K122 labeled Cu azurin. The equation used was* $G(\tau) = G_{diff}(\tau)\, G_1(\tau)\, G_2(\tau)$ *with* $\tau_D = 12$ *ms. Shown are, as function of ascorbate concentration:* F_1 *(A),* τ_1 *(B),* F_2 *(C), and* τ_2 *(D).*

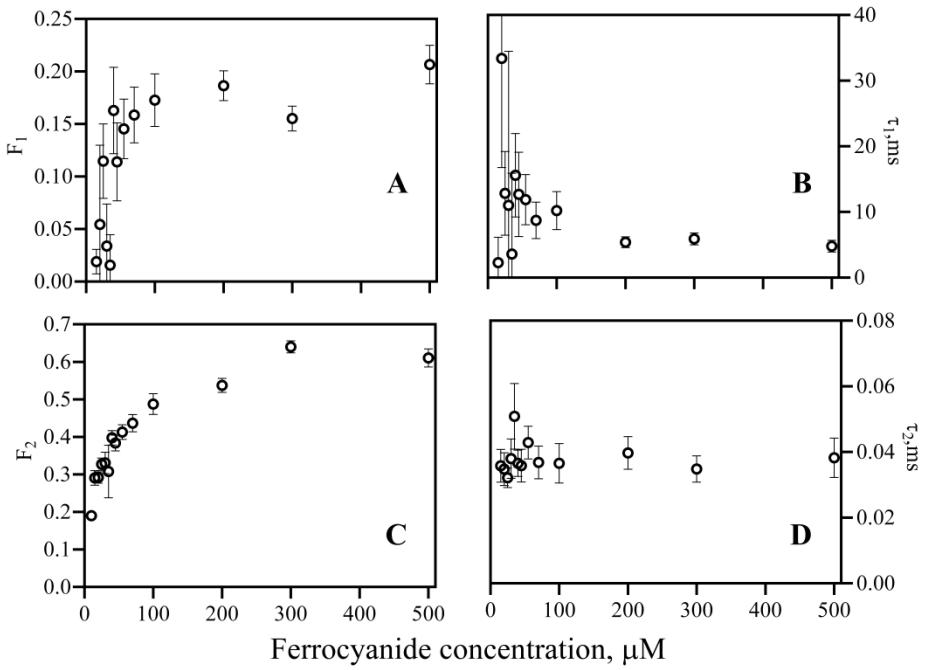

Figure 4.15: *Parameters obtained from the fits of the ACFs of K122 labeled Cu azurin. The equation used was* $G(\tau) = G_{diff}(\tau)\, G_1(\tau)\, G_2(\tau)$ *with* τ_D *=12 ms. Shown are, as function of potassium hexacyanoferrate (II) concentration:* F_1 *(A),* τ_1 *(B),* F_2 *(C), and* τ_2 *(D).*

$$LCu(I) \underset{k_{10}}{\overset{k_{01}}{\rightleftharpoons}} L^*Cu(I) \xrightarrow{k_2^f} L^-Cu(II) \xrightarrow{k_2^b} LCu(I)$$

Scheme 4.3: *Light induced ET reactions in reduced CuAz. Symbols have the same meaning as in Scheme 2. The rates for intramolecular ET from Cu(I) to L* and from L¯ to Cu(II) to are denoted by* k_2^f *and* k_2^b.

Again, consistent with the intramolecular character of the reaction, τ_2 appears independent from the reductant concentration. What seems at variance with this explanation is that the fraction of dark molecules F_2, increases with reductant concentration. We ascribe this to the oxygen present in the solution. Small amounts of reductant will be partly oxidized, which results in incomplete reduction of azurin. The ratio between reduced and oxidized protein will gradually shift towards reduced azurin as the amount of added reductant is increased. When the protein is oxidized, fluorescence from the label is reduced by FRET to the Cu site, whereas for reduced azurin the fluorescence of the label is not affected by FRET. Consequently, when both reduced and oxidized azurin are present in the solution, the expression for the ACF has to be slightly modified according to Eqn. (4.9) (The derivation of Eqn. 4.9 is shown in 'Appendix' of this

chapter)

$$G(\tau) \propto \frac{1}{\langle N \rangle} G_{diff}(\tau) G_1(\tau)(1 + \beta K e^{-\tau/\tau_2}) \qquad (4.9)$$

with $K = F_{2,red}/(1-F_{2,red})$ and β a numerical parameter between 0 and 1 depending on the ratio between the concentrations of oxidized and reduced azurin. For a 100% reduced or 100% oxidized solution β equals 1 or 0, respectively.

Eqn. (4.9) is similar to the equations (Eqn. 4.1-4.5) that were used to fit the data of K122-labeled CuAz except for the factor β. It is clear now why F_2 as obtained from the fits is not constant. This is because the fit equation did not contain β, which depends on the redox potential of the solution. Since the experimental setup did not allow for control of the latter parameter, a detailed analysis of the data in Fig. 4.14C and 4.15C is not possible. However, assuming that at 500 µM of reductant, β is close to its asymptotic value of 1, it follows that $K = F_2/(1-F_2) = 1.5 \pm 0.3$ (Fig. 4.16). Applying the same analysis as before one obtains

$F_2/\tau_2 = f(I)\ k_2^f$ and

$(1-F_2)/\tau_2 = k_2^b$

With $F_2 = 0.6$, $\tau_2 = 30$ µs and $f(I) = 4.8\times10^{-3}$ one finds $k_2^f = 4.2\times10^6$ s^{-1} and $k_2^b = 1.3\times10^4$ s^{-1}.

Now, one might wonder why F_1 is independent of oxidant concentration in Fig. 4.9 while the data for F_2 in Fig. 4.14 and 4.15 show a pronounced curvature. The reason is that the midpoint potential of the hexacyanoferrate(II)/hexacyanoferrate(III) couple (430 mV vs NHE(*43*), pH 7.0, 100 mM ionic strength) is much higher than the azurin midpoint potential (270-330 mV vs. NHE depending on pH). Azurin will be readily oxidized when hexacyanoferrate (III) is added to the sample, and thus keeping the protein close to 100% oxidized is relatively simple and F_1 will be constant. Keeping the protein reduced by employing hexacyanoferrate(II), on the other hand, requires a relatively large excess of reductant in order to lower the solution potential far enough. Even then, the oxygen in the sample will gradually raise the potential back, resulting in partial back oxidation of the reduced protein.

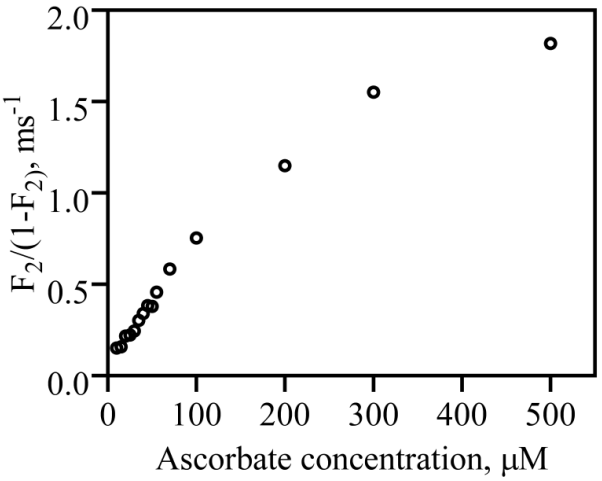

Figure 4.16: *Plot of $K= F_{2,red}/(1-F_{2,red})$ as a function of ascorbate concentrations. Kinetic parameters were obtained from the fitting of the ACFs for K122 labeled Cu azurin under reducing conditions (ascorbate). The equation used was $G(\tau) = G_{diff}(\tau)\, G_1(\tau)\, G_2(\tau)$ with τ_D =12 ms.*

Thus, F_2 will be constant only when a large excess of reductant is employed. As Fig. 4.14 or 4.15 demonstrates, this regime appears to be reached when the reductant concentration amounts to 0.5 mM or more. Again, from the forward and backward ET rates of $k_2^f = 4.2\times10^6$ s^{-1} and $k_2^b = 1.3\times10^4$ s^{-1} a value for the reorganization energy of the ET reaction can be extracted. The data obtained with ascorbate instead of hexacyanoferrate (II) were analyzed in a similar way. The resulting intramolecular ET rates are presented in Table 4.1. With $E_{ATTO/ATTO-}$ = -0.17 V (vs NHE), $n_{ATTO} = 0$ and $n_{Cu(I)}=1$ and the same values as above for the other parameters one obtains ΔG_f = -1.67 eV, ΔG_b = -0.19 eV and λ= 1.16 eV. The latter value is slightly higher than the theoretically expected value (0.95 eV).

Finally, $G_1(\tau)$ is related to the reduction of the label by the reductant and F_1 and τ_1 are analyzed as before, taking into account that only a fraction $(1-F_2)$ of the labeled molecules is in the bright state. The analysis is presented in the Fig. 4.17 and data are gathered in Table 4.1. The observed rates (k_b) are good agreement with the back oxidation rates of labeled Zn-Azurin obtained previously under redox conditions (see Chapter 3, page 90-91), since the non-fluorescent (reduced) labeled molecules have the bimolecular reactions with oxygen in a diffusion-controlled manner.

Intermolecular ET					
	Label at	$k_f f(I)^{(a)}, M^{-1}s^{-1}$	$k_f f(I)^{(b)}, M^{-1}s^{-1}$	$k_b^{(a)}, s^{-1}$	$k_b^{(b)}, s^{-1}$
CuAzurin	**N-term**	$(7.0\pm0.4)\times10^5$	$(3.2\pm0.3)\times10^5$	$(4.2\pm0.1)\times10^1$	$(3.5\pm0.2)\times10^1$
	K122	$(4.2\pm0.3)\times10^5$	$(2.0\pm0.3)\times10^5$	$(9.7\pm0.9)\times10^1$	$(5.6\pm0.6)\times10^1$
Intramolecular ET					
	Label at	$k_1^f, s^{-1(c)}$	$k_1^b, s^{-1(c)}$	$k_2^f, s^{-1(d)}$	$k_2^b, s^{-1(d)}$
CuAzurin	**K122**	$(4.8\pm0.3)\times10^4$	$(0.7\pm0.1)\times10^3$	$(3.3\pm0.7)\times10^6$	$(1.0\pm0.2)\times10^4$
		-	-	(e) $(2.2\pm0.1)\times10^6$	(e) $(1.4\pm0.1)\times10^4$

Table 4.1: *Experimental values of inter- and intramolecular ET rate constants. See text for further explanations.*

(a) hexacyanoferrate (II),

(b) ascorbate,

(c) in presence of excess of hexacyanoferrate (III),

(d) in presence of excess of ascorbate and

(e) in presence of excess of hexacyanoferrrate (II).

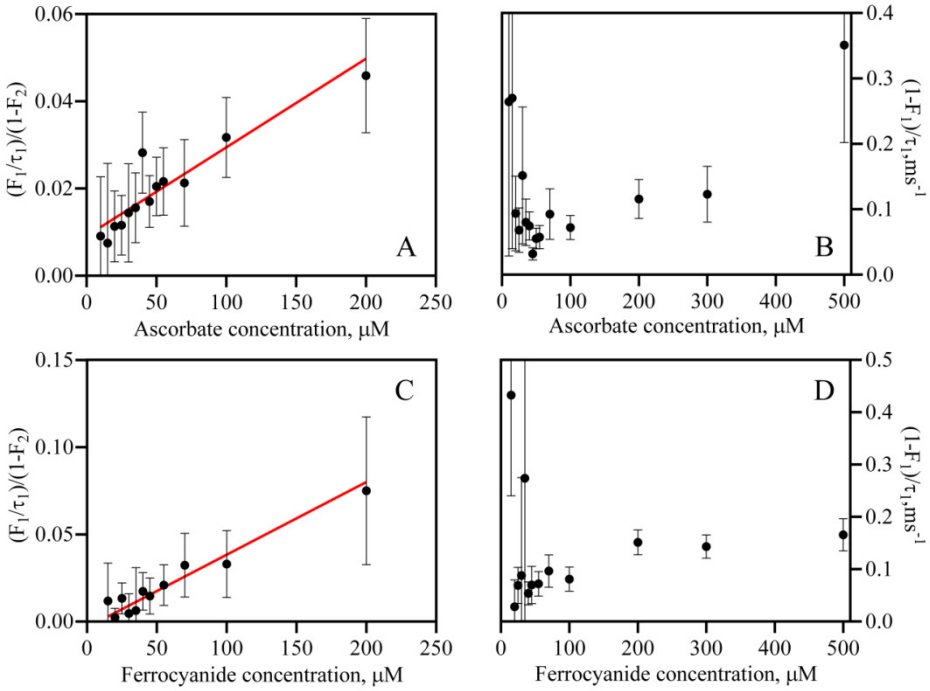

Figure 4.17: *Analysis of the ACFs of K122-labeled Cu azurin. ACFs were fitted with Eqn. 4.1 $G(\tau) = G(0)\, Gdiff(\tau)\, G_1(\tau)\, G_2(\tau)$ with τ_D =12 ms. A. Parameters τ_1 and F_1, as obtained from the fits, correspond with $G1(\tau)$. A and C: $(F_1/\tau_1)/(1-F_2)$ (k_f) as a function of the concentration of ascorbate (A) or hexacyanoferrate(II) (C); B and D: $(1-F_1)/\tau_1$ (k_b) as a function of the concentration of ascorbate (B) or hexacyanoferrate(II) (D). The red straight lines are least-squares fits to the data points.*

4.3.3.3 *ET reactions in K122-Cu Azurin as a function of viscosity*

FCS studies were performed on K122-labeled CuAzurin under 100 µM ascorbate or potassium hexacyanoferrate (II) as a function of viscosity of the solution. The buffer was kept at 20 mM HEPES pH 7.0 and the sucrose concentration was varied from 0 – 70% (w/v) in the buffer. When using highly viscous solvent, diffusion of the labeled molecule will slow down to the millisecond time scale whereas the intramolecular ET reactions between the copper and the label would remain (Fig. 4.18). ET rates do not depend on the viscosity of the solvent.

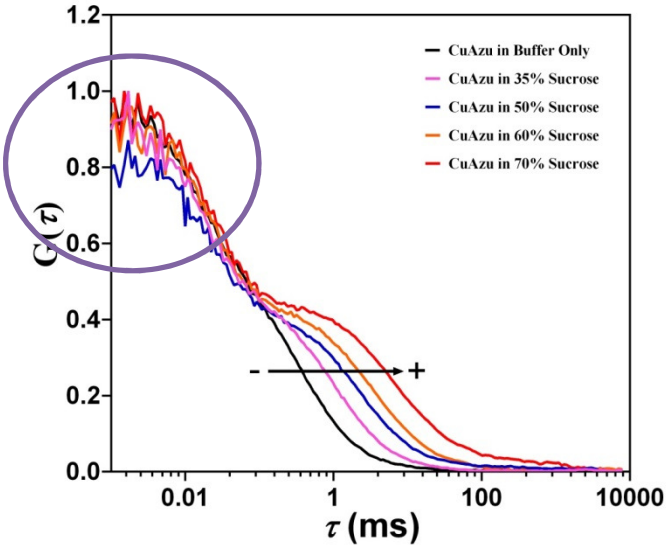

Figure 4.18: *ACFs of K122 labeled Cu-Azurin measured in the presence of 100 µM ascorbate at different concentration of sucrose solutions. The diffusion decay shifts toward longer times, whereas the decay in the sub-millisecond time range, attributed to the intramolecular electron-transfer reaction, does not shift when the viscosity is increased. The circled region represents the fraction of molecules associated with the intramolecular ET reaction.*

4.3.3.4 *Light intensity dependence of ET reactions*

Photoinduced electron transfer is supposed to be a monophotonic process. During the laser pulse, part of the ground-state molecules are pumped into the lowest excited-singlet state, and the kinetics among the thermally equilibrated lowest excited-singlet and triplet or dark states can be described by the Jablonski diagram of Chapter 1.

As mentioned earlier in this chapter, the power used for the FCS measurements is 20 µW, as measured after the objective, corresponding to a specific power of ~4.3 kW/cm^2 at the sample.

In this study, to understand the effect of laser intensity on the photoinduced intramolecular electron transfer reaction in K122 labeled CuAzurin under reducing conditions, the laser power was varied from 1 µW to 80 µW (Fig. 4.19). Then, the ACFs were analyzed according to Eqn. 4.1 with $G(\tau)= G_{diff}(\tau)\, G_1(\tau)\, G_2(\tau)$ with τ_D =12 ms. Variation of F_1, τ_1, F_2, and τ_2 as a function of laser power is shown in Fig. 4.20. Some qualitative statements can be made depending on the results.

Under redox conditions, these excited molecules react with ascorbate or hexacyanoferrate (II) and enter into dark states. These states have longer lifetimes than that of the excited dye. The process of pumping ground-state molecules into their excited states is directly related to the absorption of the ground-

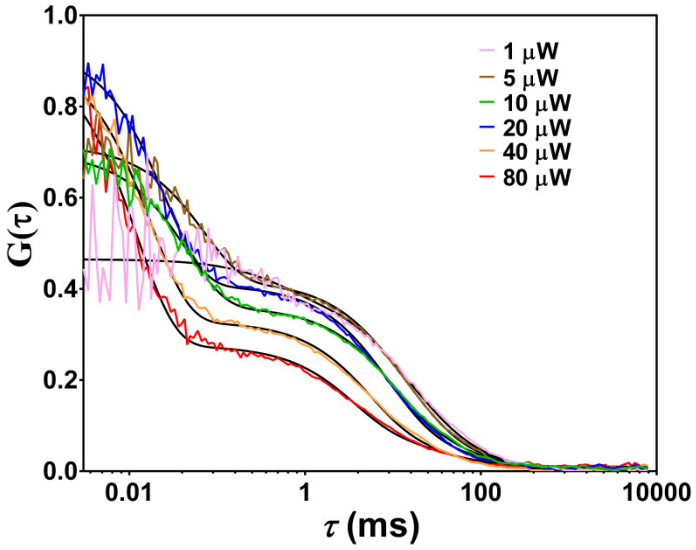

Figure 4.19: *ACFs of K122 labeled Cu-azurin measured in the presence of 100 µM ascorbate at different laser power in 70% (w/v) sucrose solution. For fitting, the equation used was* $G(\tau) = G_{diff}(\tau)\, G_1(\tau)\, G_2(\tau)$ *with* τ_D *=12 ms. The black lines are the fit according to the same equation.*

state molecules, i.e. excitation of the labeled molecules by the pulsed laser. Under high excitation power, more molecules are excited and become available for the reaction with reducing agents. As a result, intramolecular ET between the reduced label and the copper center is observed. The fraction (F_2) of labeled azurin associated with ET reaction becomes saturated at ~ 70% (transitions into dark states for ET reactions) and τ_2 becomes 20-30 µsec at higher laser power. At very low laser power (1µW), either ET reaction is absent or it is negligible. Hence, the data

points with low τ_1 and τ_2 values at the lowest laser power are not present in Fig. 4.20 and Fig. 4.21. The fraction (F_1) of molecules associated with blinking was found to be 0.2. The excitation power of the laser beam and the time scale of intramolecular reaction (τ_2) under reducing conditions are related in the following ways (Chapter 3 for details):

$$F_2/\tau_2 = f(I)\ k_2^f$$

$$\text{and } f(I) = \frac{k_{01}}{k_{10} + k_{01}}$$

where $k_{01}=\sigma I_{exc}$, with σ the absorption cross section of the label at the wavelength of the laser and I_{exc} the laser power in terms of number of photons/sec cm^2 and k_{10} is the decay rate of the excited state. Increasing excitation intensities lead to a proportional increase in the emitted fluorescence intensity. The occurrence of the factor *f(I)* can be understood by considering that the optically excited label reacts with reductant in the solution on a timescale that is long compared with the excitation and fluorescence time scales (k_{01}^{-1} and k_{10}^{-1}). For simplicity, a plot of τ_2 as a function of (1/laser power) is presented. It reports their linear relationship with a positive slope (Fig. 4.21).

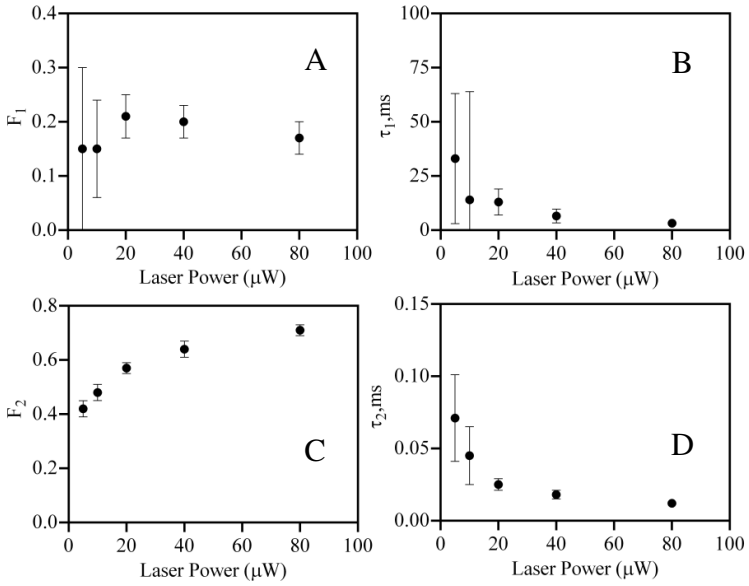

Figure 4.20: *Parameters obtained from the fits of the ACFs of K122 labeled Cu-Azurin under reducing conditions as a function of laser intensities. The equation used was $G(\tau) = G_{diff}(\tau)\ G_1(\tau)\ G_2(\tau)$ with τ_D =12 ms. Shown are, as function of laser power: F_1 (A), τ_1 (B), F_1 (C), and τ_2 (D). Data obtained at 1 μW laser power was neglected due to negligible ET rate.*

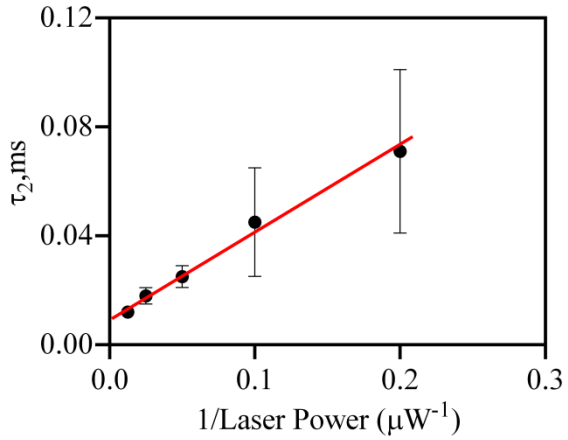

Figure 4.21: *Plot of experimentally obtained intramolecular electron transfer time scales (τ_2) as a function of (1/laser power) under reducing conditions (100 μM ascorbate) for K122-CuAzu in 70% (w/v) sucrose solution. Data obtained at 1 μW laser power was neglected due to negligible ET rate.*

4.4 *Concluding remarks*

The first conclusion from the present work is that no PET reactions with amino acids in the protein are observed, but PET to the metal is observed when Cu occupies the active site, and the label is attached close enough to the metal center (at Lys122). It means that a judicious choice of the attachment point for the label on the protein surface can diminish the effect of PET reactions on the fluorescence time trace of a single molecule. The distance between label and active center will also affect the FRET and thereby the switching ratio (*SR*), defined as:

$$SR = \frac{F_{red} - F_{ox}}{F_{red}}$$

Here F_{red} and F_{ox} are the emission intensities of the label when the protein is in the reduced (bright) and oxidized (dim) state, respectively. A high switching ratio is desirable when the label fluorescence is used to monitor the enzyme's activity. As the example of the present study shows, increasing the distance between Cu and the attachment point of the label from 18.5 to 29.1 Å abolishes PET, while it reduces the switching ratio only from ~86 to ~65% (Fig. 4.3).

Secondly, the excited label may react with redox-active components in the solution in a diffusion-controlled manner(*44*)(*45*). In the case of ATTO655 the reactions occur when there are reductants present in solution. The diffusion rates were diminished by two orders of magnitude

by increasing the viscosity. In this way the intermolecular ET reactions between label and reductant could be singled out from the intramolecular events.

Analysis of the (intramolecular) PET reactions provided values of the driving forces and the reorganization energies for the ET reactions between label and Cu center. The electronic coupling matrix elements between label and center can now be calculated. Assuming a covalent pathway for ET and expressing the electronic coupling in terms of the number of equivalent C-C bonds between Cu and label, the Marcus equation can be written as(*19*)(*36*)(*46*)(*47*)(*48*)

$$k_{ET} = 3 \times 10^{13} e^{-\beta_0 \sigma_C \ell} e^{-\frac{(\Delta G_f + \lambda)^2}{4\lambda kT}} \qquad (4.10)$$

with β_0 an attenuation factor (0.7 Å^{-1}), ℓ the length of a C-C bond (1.4 Å) and σ the number of equivalent C-C bonds in the path. Using the values of G_f and λ reported above one obtains a number of 12 or 17 equivalent bonds (Scheme 4.2 or 4.3, respectively). The actual number of bonds, depending on where the linker is considered to end and the fluorophore begins is between 13 to 17 bonds (Fig. 4.22).[1] A quantum-chemical calculation of the ground and excited state wave functions of the label, which might give more transparency on this point, is beyond the scope of the present work. The experimental data appear compatible with ET through a covalent pathway between Cu and label.

It is conceivable that instead of using a covalent pathway the electron jumps through space from the label to the protein and vice versa so that the electronic coupling will be sensitive to the motion of the label. In that case the ET rate may be expected to vary with the viscosity of the solution. In preliminary experiments where the viscosity was varied over almost two orders of magnitude the ET rate stayed constant within a factor of two (Fig. 4.18) compatible with the prevalence of a covalent pathway.

The electrostatic work term in Eqn. (4.8) contributes an amount of +144 meV (Scheme 2) or -288 meV (Scheme 3) to the driving force and eventually contributes an amount of 60 meV (Scheme 2) or – 210 meV (Scheme 3) to λ. In both cases this gives a slightly better agreement

[1] The most direct pathway between Cu and label consists of Cu–SδCγCβCα(Met121)–CαCβCγCδCεNη(Lys122)(4C)–N_{het}ATTO 655. These are 15 bonds, if we consider the Cu-S link as a bond and not as a through space jump.

with the expected value for λ (950 meV) than when the electrostatic term would have been neglected. The work term was evaluated by setting the distance between donor and acceptor at 10Å, which is the distance between Cu and the aromatic part of the label when the ATTO655 moiety is modelled as lying against the protein surface in the K122 labeled Azu variant. In this configuration the effective ε will be intermediate between that of the pure protein (ε = 4) and that of water (ε = 86)(*49*)(*50*). For obtaining an order of magnitude estimate of the possible effect of including the electrostatic work term in the calculations, the relative dielectric constant was set at 10. The numbers are only rough estimates but the calculation illustrates what effect the inclusion of the electrostatic work terms may have on the final outcome.

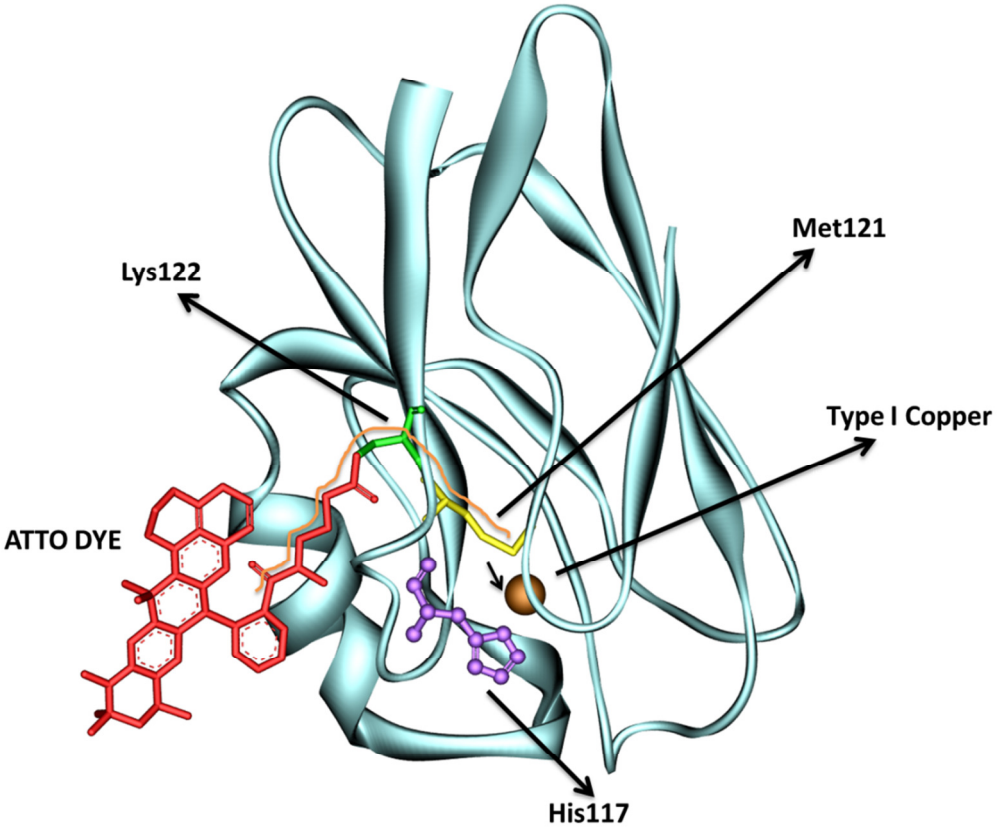

Figure 4.22: *Close-up of azurin labeled at lys122 (green) with ATTO655 (red). Type I copper is shown as a brown sphere, Met121 is shown in yellow and a small arrow points to the space between the copper and Met121 amino acid. An orange curved line has been drawn to display the most direct pathway between Cu and label consisting of Cu–SδCγCβCα(Met121)–CαCβCγCδCεNη(Lys122)(4C)–N_{het}ATTO 655. These are 15 bonds, if we consider the Cu-S link as a bond and not as a through space jump.*

The overall conclusion of the present study is that in oxido-reductases photoinduced intra-molecular ET between label and active center may occur and is not restricted to situations where the label is in Van-der-Waals contact with the redox center. This differs from instances where PET involving aromatic residues was studied and Van der Waals contact was considered a requirement for PET to occur(*51*)(*52*)(*53*)(*54*)(*55*)(*56*). The necessity for Van der Waals contact in these cases probably reflects the much lower driving force for ET due to the unfavorable midpoint potential of the aromatic residues. It is clear that for labeled oxido-reductases PET between dye and redox center can be avoided by making the distance between these large enough. The present work shows that simple thermodynamic considerations combined with ET calculations can provide a good estimate of the chances that PET may occur, and may help in designing experiments for single-molecule studies of oxido-reductases.

Although so far we have only dealt with proteins labeled via lysines or the N-terminus, the conclusions may be expected to apply equally well when (engineered) cysteines are used as anchoring points for labels.

References

(1) Chen, P.; Andoy, N. M. Single-molecule fluorescence studies from a bioinorganic perspective. *Inorganica Chim. Acta* **2008**, *361*, 809–819.

(2) Chi, Q.; Farver, O.; Ulstrup, J. Long-range protein electron transfer observed at the single-molecule level : In situ mapping of redox-gated tunneling resonance. *Proc. Natl. Acad. Sci. U. S. A.* **2005**, 16203–16208.

(3) Wang, Q.; Goldsmith, R. H.; Jiang, Y.; Bockenhauer, S. D.; Moerner, W. E. Probing single biomolecules in solution using the anti-Brownian electrokinetic (ABEL) trap. *Acc. Chem. Res.* **2012**, *45*, 1955–64.

(4) Zhang, J.; Grubb, M.; Hansen, A. G. Electron transfer behaviour of biological macromolecules towards the single-molecule level. *1873*.

(5) Zhang, J.; Chi, Q.; Hansen, A. G.; Jensen, P. S.; Salvatore, P.; Ulstrup, J. Interfacial electrochemical electron transfer in biology - towards the level of the single molecule. *FEBS Lett.* **2012**, *586*, 526–35.

(6) Chung, Y.-H.; Lee, T.; Park, H. J.; Yun, W. S.; Min, J.; Choi, J.-W. Nanoscale biomemory composed of recombinant azurin on a nanogap electrode. *Nanotechnology* **2013**, *24*,

365301.

(7) Artés, J. M.; López-Martínez, M.; Giraudet, A.; Díez-Pérez, I.; Sanz, F.; Gorostiza, P. Current-voltage characteristics and transition voltage spectroscopy of individual redox proteins. *J. Am. Chem. Soc.* **2012**, *134*, 20218–21.

(8) Schmauder, R.; Librizzi, F.; Canters, G. W.; Schmidt, T.; Aartsma, T. J. The oxidation state of a protein observed molecule-by-molecule. *Chemphyschem* **2005**, *6*, 1381–6.

(9) Kuznetsova, S.; Zauner, G.; Aartsma, T. J.; Engelkamp, H.; Hatzakis, N.; Rowan, A. E.; Nolte, R. J. M.; Christianen, P. C. M.; Canters, G. W. The enzyme mechanism of nitrite reductase studied at single-molecule level. *Proc. Natl. Acad. Sci. U. S. A.* **2008**, *105*, 3250–3255.

(10) Tabares, L. C.; Kostrz, D.; Elmalk, A.; Andreoni, A.; Dennison, C.; Aartsma, T. J.; Canters, G. W. Fluorescence lifetime analysis of nitrite reductase from Alcaligenes xylosoxidans at the single-molecule level reveals the enzyme mechanism. *Chemistry* **2011**, *17*, 12015–9.

(11) Schmauder, R.; Alagaratnam, S.; Chan, C.; Schmidt, T.; Canters, G. W.; Aartsma, T. J. Sensitive detection of the redox state of copper proteins using fluorescence. *J. Biol. Inorg. Chem.* **2005**, *10*, 683–687.

(12) Kuznetsova, S.; Zauner, G.; Schmauder, R.; Mayboroda, O. A.; Deelder, A. M.; Aartsma, T. J.; Canters, G. W. A Förster-resonance-energy transfer-based method for fluorescence detection of the protein redox state. *Anal. Biochem.* **2006**, *350*, 52–60.

(13) Tabares, L.; Gupta, A.; Aartsma, T.; Canters, G. Tracking Electrons in Biological Macromolecules: From Ensemble to Single Molecule. *Molecules* **2014**, *19*, 11660–11678.

(14) Doose, S.; Neuweiler, H.; Sauer, M. A close look at fluorescence quenching of organic dyes by tryptophan. *Chemphyschem* **2005**, *6*, 2277–85.

(15) Michalet, X.; Weiss, S.; Jäger, M. Single-Molecule Fluorescence Studies of Protein Folding and Conformational Dynamics. *Chem. Rev.* **2006**, *106*, 1785–1813.

(16) Furukawa, Y.; Ban, T.; Hamada, D.; Ishimori, K.; Goto, Y.; Morishima, I. Electron transfer reaction in a single protein molecule observed by total internal reflection fluorescence microscopy. *J. Am. Chem. Soc.* **2005**, *127*, 2098–2103.

(17) Doose, S.; Neuweiler, H.; Sauer, M. Fluorescence quenching by photoinduced electron transfer: A reporter for conformational dynamics of macromolecules. *ChemPhysChem* **2009**, *10*, 1389–1398.

(18) Gray, H. B.; Winkler, J. R. Electron tunneling through proteins. *Q. Rev. Biophys.* **2003**, *36*, 341–372.

(19) Gray, H. B.; Winkler, J. R. Electron flow through metalloproteins. *Biochim. Biophys. Acta* **2010**, *1797*, 1563–72.

(20) Winkler, J. R.; Gray, H. B. Long-range electron tunneling. *J. Am. Chem. Soc.* **2014**, *136*, 2930–2939.

(21) Gray, H. B.; Winkler, J. R.; Wiedenfeld, D. Effects of driving force on the rates of

intramolecular and bimolecular electron-transfer reactions. *Coord. Chem. Rev.* **2000**, *200–202*, 875–886.

(22) Haustein, E.; Schwille, P. Fluorescence correlation spectroscopy: novel variations of an established technique. *Annu. Rev. Biophys. Biomol. Struct.* **2007**, *36*, 151–69.

(23) Ries, J.; Schwille, P. Fluorescence correlation spectroscopy. *BioEssays* **2012**, *34*, 361–368.

(24) Haustein, E.; Schwille, P. Ultrasensitive investigations of biological systems by fluorescence correlation spectroscopy. *Methods* **2003**, *29*, 153–166.

(25) Krichevsky, O. Fluorescence correlation spectroscopy : the technique. *Rep.Prog.Phys* **2002**, *65*, 251.

(26) Felekyan, S.; Kühnemuth, R.; Kudryavtsev, V.; Sandhagen, C.; Becker, W.; Seidel, C. a M. Full correlation from picoseconds to seconds by time-resolved and time-correlated Single photon detection. *Rev. Sci. Instrum.* **2005**, *76*, 1–14.

(27) Goldberg, M.; Pecht, I. Kinetics and equilibria of the electron transfer between azurin and the hexacyanoiron (II/III) couple. *Biochemistry* **1976**, *15*, 4197–4208.

(28) Van de Kamp, M.; Hali, F. C.; Rosato, N.; Agro, A. F.; Canters, G. W. Purification and characterization of a non-reconstitutable azurin, obtained by heterologous expression of the Pseudomonas aeruginosa azu gene in Escherichia coli. *Biochim. Biophys. Acta* **1990**, *1019*, 283–292.

(29) Nicolardi, S.; Andreoni, A.; Tabares, L. C.; van der Burgt, Y. E. M.; Canters, G. W.; Deelder, A. M.; Hensbergen, P. J. Top-down FTICR MS for the identification of fluorescent labeling efficiency and specificity of the Cu-protein azurin. *Anal. Chem.* **2012**, *84*, 2512–20.

(30) E. T. Adman andL. H. Jensen Structural Features of Azurin at 2.7 Å Resolution. *Isr. J. Chem.* **1981**, *21*, 8–12.

(31) Robert C. Weast, M. J. A. *CRC Handbook of Chemistry and Physics*; CRC Press, Inc, Boca Raton, Florida.

(32) Lakowicz, J. R.; Gryczynski, I.; Laczko, G.; Gloyna, D. Picosescond fluorescence lifetime standards for frequency- and time-domain fluorescence. *J. Fluoresc.* **1991**, *1*, 87–93.

(33) Lampert, R. A.; Chewter, L. A.; Phillips, D.; O'Connor, D. V; Roberts, A. J.; Meech, S. R. Standards for nanosecond fluorescence decay time measurements. *Anal. Chem.* **1983**, *55*, 68–73.

(34) Marcus, R. a.; Sutin, N. Electron transfers in chemistry and biology. *Biochim. Biophys. Acta - Rev. Bioenerg.* **1985**, *811*, 265–322.

(35) Newton, M. Electron transfer reactions in condensed phases. **1984**, *35*, 437–480.

(36) Canters, G. W.; van de Kamp, M. Protein-mediated electron transfer. *Curr. Opin. Struct. Biol.* **1992**, *2*, 859–869.

(37) Rehm, D.; Weller, A. Kinetics of fluorescence quenching by electron and hydrogen-atom

transfer. *Isr. J. Chem.* **1970**, *8*, 259–271.

(38) Van De Kamp, M.; Canters, G. W.; Andrew, C. R.; Sanders-Loehr, J.; Bender, C. J.; Peisach, J. Effect of lysine ionization on the structure and electrochemical behaviour of the Met44-->Lys mutant of the blue-copper protein azurin from Pseudomonas aeruginosa. *Fed. Eur. Biochem. Soc. J.* **1993**, *218*, 229–238.

(39) Clair, C. S.; Ellis, W.; Gray, H. Spectroelectrochemistry of blue copper proteins: pH and temperature dependences of the reduction potentials of five azurins. *Inorganica Chim. Acta* **1992**, *191*, 149–155.

(40) Zhu, R.; Li, X.; Zhao, X. S.; Yu, A. Photophysical properties of Atto655 dye in the presence of guanosine and tryptophan in aqueous solution. *J. Phys. Chem. B* **2011**, *115*, 5001–7.

(41) Seidel, C. a. M.; Schulz, A.; Sauer, M. H. M. Nucleobase-Specific Quenching of Fluorescent Dyes. 1. Nucleobase One-Electron Redox Potentials and Their Correlation with Static and Dynamic Quenching Efficiencies. *J. Phys. Chem.* **1996**, *100*, 5541–5553.

(42) Bellion, E. The Biological Chemistry of the Elements: The Inorganic Chemistry of Life (da Silva, J. J. R. Frausto; Williams, R. J. P.). *J. Chem. Educ.* **1992**, *69*, A326.

(43) O'Reilly, J. E. Oxidation-reduction potential of the ferro-ferricyanide system in buffer solutions. *Biochim. Biophys. Acta* **1973**, *292*, 509–515.

(44) Widengren, J.; Chmyrov, A.; Eggeling, C.; Löfdahl, P.-A.; Seidel, C. A. M. Strategies to improve photostabilities in ultrasensitive fluorescence spectroscopy. *J. Phys. Chem. A* **2007**, *111*, 429–440.

(45) Vogelsang, J.; Kasper, R.; Steinhauer, C.; Person, B.; Heilemann, M.; Sauer, M.; Tinnefeld, P. A reducing and oxidizing system minimizes photobleaching and blinking of fluorescent dyes. *Angew. Chemie Int. Ed.* **2008**, *47*, 5465–5469.

(46) Onuchic, J. N.; Beratan, D. N.; Winkler, J. R.; Gray, H. B. Pathway analysis of protein electron-transfer reactions. *Annu. Rev. Biophys. Biomol. Struct.* **1992**, *21*, 349–377.

(47) Megan L. Jones, I. V. K.; Beraton, D. N. The nature of tunneling in pathway and average packing density models for protein-mediated electron transfer. **2002**, *106*, 2002–2006.

(48) D. N. Beratan; J; J. N. Betts; N; Onuchic Protein Electron Transfer Rates set by the Bridging Secondary and Tertiary Structure. *Science (80-.).* **1991**, *7*, 1285–1288.

(49) T. Simomson, C. L. B. Charge Screening and the Dielectric Constant of Proteins: Insights from Molecular Dynamics. *J. Am. Chem. Soc.* **1996**, *118*, 8452–8458.

(50) C. G. Malmberg, A. A. M. Dielectric constant of water from 0° to 100 °C. *J. Res. Natl. Bur. Stand. (1934).* **1956**, *56*, 1–8.

(51) Tanaka, F.; Chosrowjan, H.; Taniguchi, S.; Mataga, N.; Sato, K.; Nishina, Y.; Shiga, K. Donor-acceptor distance-dependence of photoinduced electron-transfer rate in flavoproteins. *J. Phys. Chem. B* **2007**, *111*, 5694–9.

(52) Porcal, G.; Bertolotti, S. G.; Previtali, C. M.; Encinas, M. V. Electron transfer quenching of singlet and triplet excited states of flavins and lumichrome by aromatic and aliphatic

electron donors. *Phys. Chem. Chem. Phys.* **2003**, *5*, 4123.

(53) Murakami, M.; Ohkubo, K.; Fukuzumi, S. Inter- And intramolecular photoinduced electron transfer of flavin derivatives with extremely small reorganization energies. *Chem. - A Eur. J.* **2010**, *16*, 7820–7832.

(54) Kang, H.; Jouvet, C.; Dedonder-Lardeux, C.; Martrenchard, S.; Charrière, C.; Grégoire, G.; Desfrançois, C.; Schermann, J. P.; Barat, M.; Fayeton, J. a Photoinduced processes in protonated tryptamine. *J. Chem. Phys.* **2005**, *122*, 84307.

(55) Grégoire, G.; Lucas, B.; Barat, M.; Fayeton, J. A.; Dedonder-Lardeux, C.; Jouvet, C. UV photoinduced dynamics in protonated aromatic amino acid. *Eur. Phys. J. D* **2009**, *51*, 109–116.

(56) Jones, G.; Farahat, C. W. Photoinduced electron and hole transfer involving eosin conjugates of tryptophan derivatives. *Res. Chem. Intermed.* **1994**, *20*, 855–877.

(57) Gupta, A.; Aartsma, T. J.; Canters, G. W. One at a time: Intramolecular electron-transfer kinetics in small laccase observed during turnover. *J. Am. Chem. Soc.* **2014**, *136*, 2707–2710.

(58) Salverda, J. M.; Patil, A. V.; Mizzon, G.; Kuznetsova, S.; Zauner, G.; Akkilic, N.; Canters, G. W.; Davis, J. J.; Heering, H. A.; Aartsma, T. J. Fluorescent Cyclic Voltammetry of Immobilized Azurin: Direct Observation of Thermodynamic and Kinetic Heterogeneity. *Angew. Chemie Int. Ed.* **2010**, *49*, 5776–5779.

Appendix

Autocorrelation function when the azurin in solution is only partly reduced in case of K122-Cu azurin

When the azurin in a sample is only partly reduced the expression for the ACF has to be adapted from what is described by Eqns. 4.1 – 4.6 previously. This can be understood by realizing that a partly reduced sample contains reduced as well as oxidized azurin molecules and that these two species exhibit different brightness. In the oxidized form FRET quenches part of the fluorescence, while in the reduced azurin the fluorescence of the label is maximal. Consequently, the expression for the ACF has to be adapted.

When denoting the relative brightness of the label in the oxidized (Cu(II)Az) and the reduced (Cu(I)Az) azurin by η_{ox} and η_{red} , respectively, and the fractions of the azurin molecules in the oxidized and reduced form by ρ_{ox} and ρ_{red}, respectively, the expression for the ACF can be derived from the more general expression in (*57*)(*58*), and it becomes:

$$G(\tau) = \frac{\eta_{ox}^2 \rho_{ox} G_{ox}(\tau) + \eta_{red}^2 \rho_{red} G_{red}(\tau)}{(\eta_{ox}\rho_{ox} + \eta_{red}\rho_{red})^2} \qquad \text{(A.1)}$$

The ACFs for the oxidized and reduced particles, $G_{ox}(\tau)$ and $G_{red}(\tau)$, respectively, each have the form of Eqn. (A.1). They are similar except for the part that corresponds with the intramolecular ET between Cu^+ and the label and between the label and Cu^{2+}. Here we ignore the latter reaction. It occurs at a much longer time scale than the former reaction and the contribution to the ACF is small unless the degree of reduction is very low which is not the case considered here. Hence $G_{2,ox} = 1$ whereas

$$G_{2,red}(\tau) = \frac{(1 - F_{2,red} + F_{2,red} e^{-\tau/\tau 2})}{(1 - F_{2,red})} \qquad \text{(A.2)}$$

The subscripts *ox* and *red* refer to the oxidized and reduced azurin molecules and the subscript 2 denotes the parts in the ACF that correspond with the ET reaction between label and Cu. After some rearrangement Eqn. A.1 becomes

$$G(\tau) = \frac{1}{\langle N \rangle} \alpha G_{diff}(\tau) G_1(\tau)(1 + \beta K e^{-\tau/\tau 2}) \qquad \text{(A.3)}$$

where,

$$K = \frac{F_{2,red}}{1 - F_{2,red}}$$

$$\alpha = \frac{\eta_{ox}^2 \rho_{ox} + \eta_{red}^2 \rho_{red}}{(\eta_{ox} \rho_{ox} + \eta_{red} \rho_{red})^2}$$

$$\beta^{-1} = 1 + (\frac{\eta_{ox}}{\eta_{red}})^2 \frac{\rho_{ox}}{\rho_{red}}$$

The Eqn. (A.2) is similar to the Eqns. (4.1)-(4.6) that were used to fit the data of K122-labeled CuAz except for the factors α and β. It is clear now why F_2 did not come out as a constant from this fit since the fit equation did not contain the factor β. Also $G(0)$ will vary with the degree of reduction when Eqns. (4.1)-(4.6) are used because of the factor α. When the reduction proceeds, ρ_{ox}/ρ_{red} diminishes and α and β will approach $1/\rho_{red}$ and 1, respectively, and become constant. It is clear that both α and β depend on the ratio between oxidized and reduced azurin, *i.e.*, on the redox potential of the solution.